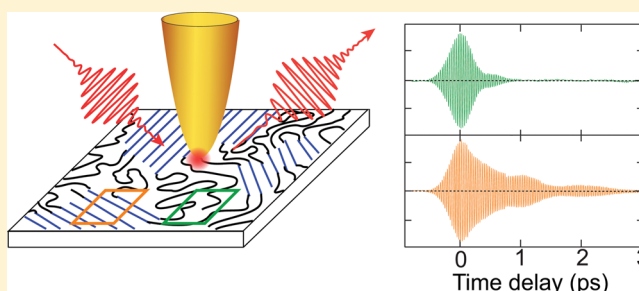


## Nanoscale Probing of Dynamics in Local Molecular Environments

Joanna M. Atkin,<sup>\*,†,‡</sup> Paul M. Sass,<sup>†,§</sup> Paul E. Teichen,<sup>||</sup> Joel D. Eaves,<sup>||</sup> and Markus B. Raschke<sup>\*,†</sup><sup>†</sup>Department of Physics, Department of Chemistry, and JILA, University of Colorado, Boulder, Colorado 80309, United States<sup>||</sup>Department of Chemistry, University of Colorado, Boulder, Colorado 80309, United States<sup>‡</sup>Department of Chemistry, University of North Carolina, Chapel Hill, North Carolina 27599, United States<sup>§</sup>Environmental and Molecular Sciences Laboratory, Pacific Northwest National Laboratory, Richland, Washington 99354, United States

## Supporting Information

**ABSTRACT:** Vibrational spectroscopy can provide information about structure, coupling, and dynamics underlying the properties of complex molecular systems. While measurements of spectral line broadening can probe local chemical environments, the spatial averaging in conventional spectroscopies limits insight into underlying heterogeneity, in particular in disordered molecular solids. Here, using femto-second infrared scattering scanning near-field optical microscopy (IR *s*-SNOM), we resolve in vibrational free-induction decay (FID) measurements a high degree of spatial heterogeneity in polytetrafluoroethylene (PTFE) as a dense molecular model system. In nanoscopic probe volumes as small as  $10^3$  vibrational oscillators, we approach the homogeneous response limit, with extended vibrational dephasing times of several picoseconds, that is, up to 10 times the inhomogeneous lifetime, and spatial average converging to the bulk ensemble response. We simulate the dynamics of relaxation with a finite set of local vibrational transitions subject to random modulations in frequency. The combined results suggest that the observed heterogeneity arises due to static and dynamic variations in the local molecular environment. This approach thus provides real-space and real-time visualization of the subensemble dynamics that define the properties of many functional materials.



Ultrafast vibrational spectroscopy provides information about molecular structure, inter- and intramolecular coupling, and associated dynamical processes. Probing in the time domain can separate competing relaxation pathways and therefore provides insight into the mechanisms underlying, for example, chemical reactions and charge and energy transfer.<sup>1,2</sup> Traditional linear and nonlinear IR vibrational spectroscopies measure the collective response from a large number (comparable to Avogadro's number) of molecular oscillators, providing only an averaged view of a molecular ensemble. While hole burning, photon echo, or coherent multidimensional implementations can access the response of a subensemble of molecules, these methods still cannot resolve whether dynamical differences in spectra emerge from spatially distinct regions of the system.<sup>3–6</sup> This is a particular challenge for the understanding of dynamically heterogeneous systems, such as multiphase, glassy, or disordered molecular systems, where molecules separated by only a few molecular diameters can already relax on vastly different time scales.<sup>7,8</sup>

Nanoscale vibrational spectroscopy beyond the diffraction limit opens a path toward resolving the dynamics of subensembles in terms of their spatial distributions. We use femtosecond IR vibrational scattering-scanning near-field optical microscopy (IR *s*-SNOM), with high temporal, spectral, and spatial resolution, to investigate the vibrational dynamics of

local nanoscopic probe volumes in spatially distinct chemical environments. In measurements of the free induction decay (FID) of  $\text{CF}_2$  oscillators in a polytetrafluoroethylene (PTFE) single-component polymer, we resolve large variations in local vibrational dynamics and the underlying nanoscale heterogeneity of the system. The broad distribution of associated line widths indicates that the sample exhibits both static and dynamic heterogeneity, with the average of all local nanoprobe measurements approaching the ensemble bulk response.

We develop a stochastic line shape theory for finite systems based on the Kubo–Anderson model, where thermal fluctuations with the environment introduce a stochastic component to each vibrational transition frequency that leads to dephasing. We find that number fluctuations only manifest in measurements that probe fewer than  $10^3$  oscillators and therefore are not an important line-broadening mechanism. This work thus provides for the first real-space and real-time insight into the origin of heterogeneity due to variations in the dynamics of the local chemical environment.

In *s*-SNOM, the tip of an atomic force microscope (AFM) is used to localize and enhance incident optical fields and scatter

Received: September 20, 2015

Accepted: November 3, 2015

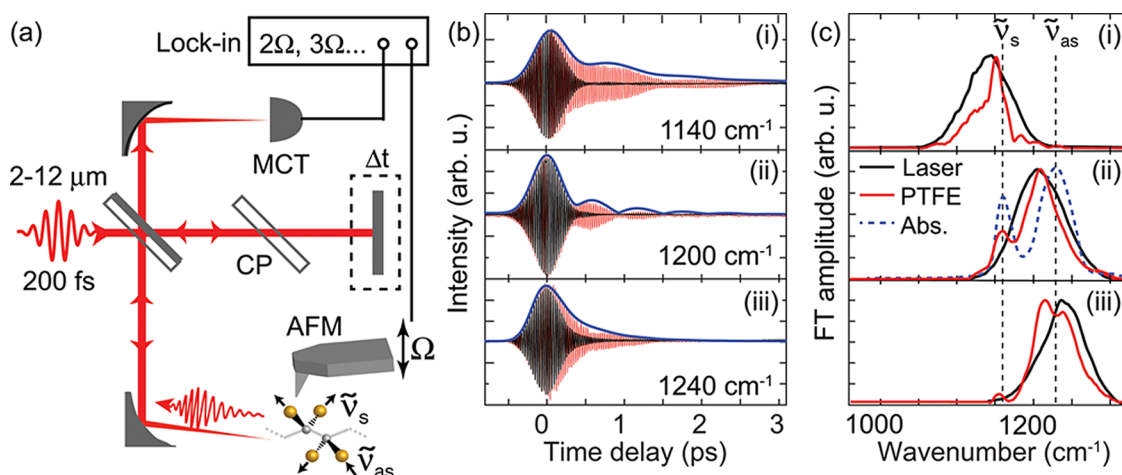


**Figure 1.** (a) Experimental schematic for femtosecond IR *s*-SNOM on PTFE, with symmetric  $\tilde{\nu}_s$  and antisymmetric  $\tilde{\nu}_{as}$  C (gray)–F (yellow) stretch modes. (b) Interferogram of laser pulse (black) and response of sample (red) for second harmonic of the cantilever oscillation  $2\Omega$ . For excitation close to a molecular vibrational resonance, free induction decay is observed. The response can be modeled with two damped, driven harmonic oscillators interfering with a background field (blue lines). (c) Fourier transforms (FTs) of the interferograms, with pulse (black) and PTFE response (red). The pulse bandwidth is  $\sim 80 \text{ cm}^{-1}$ , and spectral dips appear in the PTFE response close to the far-field PTFE absorption maxima (dashed line).

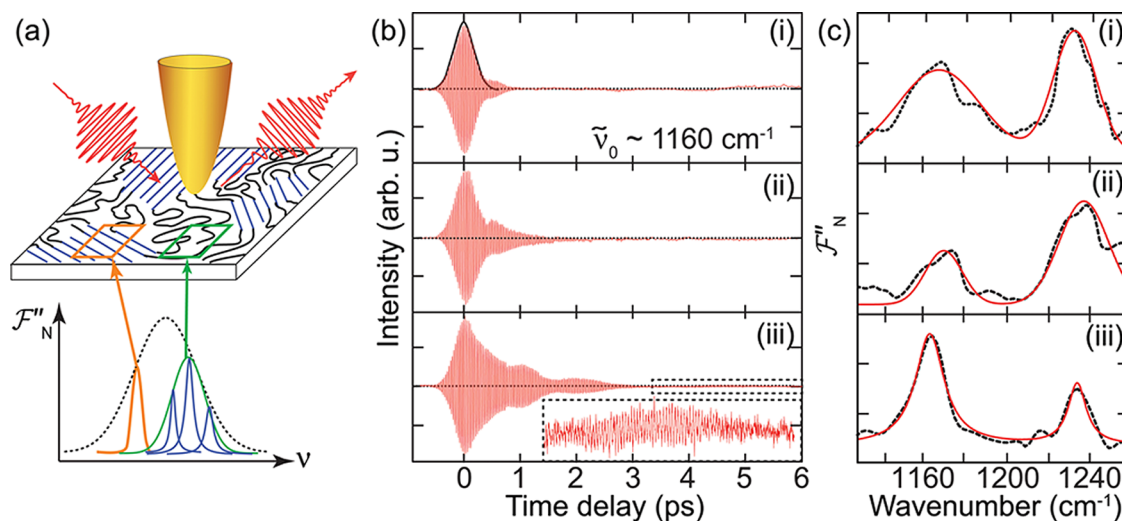


**Figure 2.** (a) Illustration of the organization of long-chain PTFE molecules. Both highly ordered (blue) and less-ordered (black) regions occur, with varying densities and orientations. The small ensemble response can reveal variations in line widths associated with the distribution of subensembles of the bulk system. (b) Time-domain variations in FID at different sample positions, for driving laser pulse  $\tilde{\nu}_0 \approx 1160 \text{ cm}^{-1}$  ( $2\Omega$ ). For one measurement (i), the initial FID envelope relaxes with dephasing time of  $\sim 1.3 \text{ ps}$ , but coherent behavior can be observed to almost 6 ps. (c) Corresponding FTs normalized to laser spectrum,  $\mathcal{F}''_N$ , showing variations in line width and spectral position, correlating with observed dephasing time (black dashed line). Gaussian (i,ii) and Lorentzian (iii) fits to  $\mathcal{F}''_N$  shown in red.

near-field radiation from nanoscale sample volumes.<sup>9,10</sup> This approach is compatible with a wide range of visible and IR spectroscopies,<sup>11–15</sup> including pump–probe spectroscopy.<sup>16,17</sup> Here we perform coherent ultrafast IR *s*-SNOM, where the sample is excited by a broadband femtosecond IR pulse tuned to a vibrational resonance to measure the real-time response (Figure 1a, for details see [Experimental Methods](#)). The tip-scattered free induction decay (FID) is resolved in the time domain by interferometric heterodyne detection and consists of a temporal superposition of the pure near-field FID with a nonresonant background. The FID response is described by the optical polarization  $P(t) = \int_0^\infty d\tau R(\tau) E(t - \tau)$ , with driving field  $E(t)$  and vibrational oscillator response  $R(t)$ . The instantaneous nonresonant response of a Au surface is used as a reference to determine  $E(t)$ .

Polytetrafluoroethylene (PTFE, Sigma-Aldrich) provides a model system, characterized by high oscillator density and a large transition dipole moment of the C–F bonds. The symmetric and antisymmetric  $\text{CF}_2$  stretch modes have frequencies of  $\tilde{\nu}_s \approx 1160 \text{ cm}^{-1}$  and  $\tilde{\nu}_{as} \approx 1220 \text{ cm}^{-1}$ , respectively, as determined from FTIR and electron energy loss spectroscopy at room temperature.<sup>18–20</sup> PTFE molecules tend to have a large average chain length and form straight segments due to the electronegativity of the F atoms. The variation in the degree of ordering across the sample and the existence of several possible crystalline phases of PTFE<sup>21</sup> are representative for many complex macromolecular systems.

Figure 1b shows the vibrational decoherence following resonant excitation of the  $\text{CF}_2$  vibrational oscillators (red), with the nonresonant near-field response from the Au surface

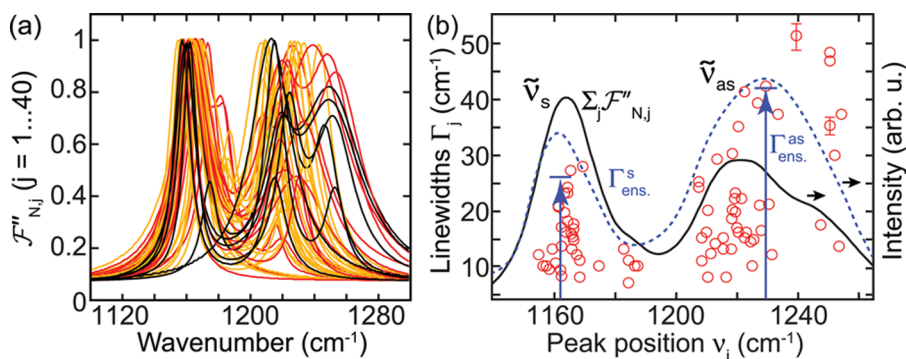


**Figure 3.** (a) Lorentzian line fits to imaginary part of the near-field signal,  $\mathcal{F}''_{N,j}$ , for all measurements at different locations and with different excitation frequencies. Black lines are for excitation frequency centered at  $\tilde{\nu}_0 \approx 1220 \text{ cm}^{-1}$ , red  $\tilde{\nu}_0 \approx 1190 \text{ cm}^{-1}$ , and orange  $\tilde{\nu}_0 \approx 1160 \text{ cm}^{-1}$ . Spectra are normalized for clarity. (b) Scatter plot showing variation in line width and peak position for the extracted Lorentzian analysis. Arrows indicate line widths  $\Gamma_{\text{ens}}^s$  and  $\Gamma_{\text{ens}}^{\text{as}}$  from far-field absorption spectrum. Sum of all normalized near-field peaks  $\sum_j \mathcal{F}''_{N,j}$  (black line) and far-field absorption spectrum (blue dashed line).

as reference (black). The corresponding spectral behavior from Fourier transform (FT) of the interferograms is shown in Figure 1c, with the excitation frequencies  $\tilde{\nu}_0 = 1140$  (i),  $1200$  (ii), and  $1240 \text{ cm}^{-1}$  (iii). The asymmetric FID interferograms have complex-valued FTs and therefore directly provide dispersive and absorptive information about the vibrational modes from the real and imaginary near-field response, respectively.<sup>11,12,14,22,23</sup> Because the response of the tip itself is spectrally flat, the tip-scattered near-field  $\mathcal{F}'_N$  (real part) and  $\mathcal{F}''_N$  (imaginary part) are related to the dielectric function of the sample  $\tilde{\epsilon} = \epsilon_1 + i\epsilon_2$ , so that  $\mathcal{F}''_N$  approximates  $\epsilon_2(\tilde{\nu})$  of the spatial absorption coefficient  $\kappa(\tilde{\nu})$ .<sup>24,25</sup> The real part exhibits a dispersive line shape, which without normalization leads to dips in the laser spectrum close to  $\tilde{\nu}_s$  and  $\tilde{\nu}_{\text{as}}$  (Figure 1c, red). A far-field FTIR absorption spectrum on PTFE is shown for comparison (blue dashed line).

The excitation spectrum, with center frequency  $\tilde{\nu}_0$ , determines the vibrational modes dominating the FID response. For  $\tilde{\nu}_0 = 1140 \text{ cm}^{-1}$  (i), we primarily drive the lower frequency, symmetric  $\tilde{\nu}_s$  mode, where we see a stronger FID response and comparatively slow relaxation, with vibrational coherence lasting as long as  $\sim 3 \text{ ps}$ . At  $\tilde{\nu}_0 = 1240 \text{ cm}^{-1}$  (iii), we primarily drive the  $\tilde{\nu}_{\text{as}}$  mode, characterized by a smaller amplitude FID response and faster relaxation. When the excitation frequency is tuned to  $\tilde{\nu}_0 = 1200 \text{ cm}^{-1}$  (ii), a beat frequency of  $\sim 50 \text{ cm}^{-1}$ , close to the spectral separation between the two modes, is observed.

The time-domain response can be simulated with two driven, damped, and uncoupled harmonic oscillators, representing  $\tilde{\nu}_s$  and  $\tilde{\nu}_{\text{as}}$ . Taking additional interference from the broadband background field into consideration reproduces the temporal response in all cases (blue line, for details see SI.)

Where in previous coherent *s*-SNOM experiments we have introduced *extrinsic* heterogeneities in the form of metallic nanostructures to modify the dephasing dynamics and investigate the fundamental properties of the near-field response,<sup>23,26</sup> the improved IR source stability, higher detection sensitivity, and spectral and temporal resolution in this experiment allow us to probe the true subensemble dynamics and access the *intrinsic* inhomogeneities of the molecular system. In our experiments, we estimate a lateral spatial resolution of  $\sim 10 \text{ nm}$  based on approach curves and spatial scans (details in supplement). This corresponds to ensembles on the order of  $10^3$  to  $10^4$  vibrational oscillators in PTFE. We

are therefore able to probe small regions of a bulk sample to investigate spatial variations, subensemble dynamics, and the origins of line-broadening, as illustrated in Figure 2a.

On the basis of far-field absorption spectra, we can estimate a heterogeneous ensemble dephasing time for  $\tilde{\nu}_s$  of  $680 \pm 50 \text{ fs}$  and  $340 \pm 40 \text{ fs}$  for  $\tilde{\nu}_{\text{as}}$ . Figure 2b shows three examples of near-field dephasing times, observed at different sample positions with the same driving field, with center frequency  $\sim 1160 \text{ cm}^{-1}$ . While repeated measurements in the same spatial position are highly reproducible in terms of dephasing time and beating behavior, different sample locations show—in part large—variations in both the oscillating frequency and decay times of the FID. From the near-field measurements, we can directly observe dephasing times ranging from as short as  $500 \text{ fs}$ , that is, comparable to the ensemble response, up to as long as several picoseconds. Additionally, for a subset ( $\sim 10\%$ ) of FID measurements we observe long extended coherence times after the initial faster exponential relaxation behavior (iii). Here the initial FID shows a dephasing time of  $\sim 1.3 \text{ ps}$  but with coherence persisting to  $\geq 6 \text{ ps}$  (magnified inset in (iii)). Notably, these long time scale coherences contain the same vibrational frequency components as the initial FID.

Although the tip can modify the local environment through distortion of the driving field and introduction of additional coupling and dephasing pathways, measurements with different tip-sample separations suggest that this effect is minimal for the excitation regime in these experiments (Figure S4). Furthermore, a tip-induced enhancement in the radiative emission rate would lead to an increase in the dephasing rate,<sup>23</sup> opposite to the longer coherence times observed here. (In contrast with the case of fluorescence with nanosecond radiative lifetimes, modification of intrinsic subpicosecond coherent dynamics requires stronger coupling of the emitter to antenna or plasmonic metal nanostructure.<sup>23,26</sup>)

The normalized imaginary part of the FTs,  $\mathcal{F}''_N$ , associated with the variable dephasing times is shown in Figure 2c. Line fits to the near-field spectra are shown in red. For the case of long dephasing times (iii), the line shape is narrower and Lorentzian, while for the shorter dephasing times a broader and more Gaussian line shape is observed.

The results of corresponding Lorentzian peak fits to  $\mathcal{F}''_{N,j}$ , for 40 different *s*-SNOM FID measurements  $j = 1..40$  at different sample locations within a  $2 \mu\text{m} \times 2 \mu\text{m}$  area, are

shown in Figure 3a. The *s*-SNOM signal varies over the measured area, with weak correlation with the topography (Figure S3). The coherence lifetime in different locations does not coincide with a high (or low) *s*-SNOM or FID signal, similar to observations in disordered plasmonic systems<sup>27</sup> yet with a reproducible spectral response for repeated measurements in the same spatial position. The spectra exhibit a distribution of center frequencies  $\tilde{\nu}_i$  and line widths  $\Gamma_j$  for the  $\tilde{\nu}_s$  and  $\tilde{\nu}_{as}$  CF<sub>2</sub> modes, as shown in Figure 3b. We observe consistently narrower line widths for both CF<sub>2</sub> modes for the local probe measurements, compared with the bulk response with  $\Gamma_{ens}^s = 26 \text{ cm}^{-1}$  and  $\Gamma_{ens}^{as} = 42 \text{ cm}^{-1}$ . For  $\tilde{\nu}_s$  the center frequencies vary by  $>20 \text{ cm}^{-1}$ , and the line widths vary from  $<10$  to  $30 \text{ cm}^{-1}$ . For  $\tilde{\nu}_{as}$ , the variation in center frequency is even larger, with  $\Gamma_j^{as}$  from  $<10$  to  $>40 \text{ cm}^{-1}$ . The narrowest line widths extracted for  $\tilde{\nu}_s$  and  $\tilde{\nu}_{as}$  approach the homogeneous limit, while the widest are comparable to the bulk values for the respective vibrational modes. The wider distribution for  $\Gamma_j^{as}$  is consistent with results from bulk measurements, with a typically broader line shape for  $\tilde{\nu}_{as}$  than  $\tilde{\nu}_s$  and with center frequency and line width varying with sample preparation.<sup>18,21,28,29</sup> The averaged response of all local probe measurements (black line) approaches the bulk FTIR spectrum (blue dashed line), suggesting that through *s*-SNOM we are probing the *intrinsic* spatial, spectral, and temporal molecular response and decomposition of the heterogeneous bulk ensemble response.

There are several sources of line broadening that can contribute to our observed variations in line widths. One possible contribution is fluctuations in the number of oscillators probed within small near-field sample volumes. To model the effect of these number fluctuations, we apply a stochastic version of the Kubo–Anderson line shape theory.<sup>30–33</sup> In this model, the vibrational lifetime is long, and the interactions with the surrounding chemical environment causes a stochastic modulation of the frequency between a single PTFE oscillator so that relaxation occurs through dephasing alone. The vibrational frequency becomes time-dependent,  $\nu(t) = \tilde{\nu} + \delta\nu(t)$ , where  $\tilde{\nu}$  is the mean vibrational frequency and  $\delta\nu(t)$  is the fluctuating part with zero mean. In the ensemble limit, the spectral line shape depends only on the frequency–frequency time correlation function,  $C(t) = \langle \delta\nu(t)\delta\nu(0) \rangle$ , with  $C(t) = \Delta^2 \exp(-t/\tau)$  in the Kubo–Anderson model. The two parameters in this theory are the root-mean-squared strength of the frequency fluctuations  $\Delta$  and the decay rate of the vibrational frequency fluctuations  $1/\tau$ . This theory can capture both the inhomogeneous, static limit ( $\Delta\tau \gg 1$ ), and the homogeneous limit ( $\Delta\tau \ll 1$ ) of the spectral fluctuation dynamics. The absorption spectrum is proportional to

$$I(\nu - \tilde{\nu}) \propto \int_{-\infty}^{\infty} dt e^{-i2\pi\tilde{\nu}t} \text{Re}[G(t)] \quad (1)$$

with the dissipative propagator

$$G(t) \equiv \langle \exp(-i \int_0^t ds \delta\nu(s)) \rangle \quad (2)$$

In the ensemble limit, where  $N \rightarrow \infty$  and Gaussian statistics hold,  $G(t) = \exp(-\int_0^t ds (t-s)C(s))$ . While  $G(t)$  is formally an ensemble average, the form in eq 2 provides a straightforward generalization for also simulating the vibrational spectral dynamics for a finite system<sup>34</sup> by replacing the ensemble average with an average over a finite number of stochastic trajectories for  $\delta\nu(t)$ .

We simulate  $N$  stochastic realizations of the time-dependent fluctuations,  $\delta\nu(t)$ , using the Langevin equation

$$\frac{d}{dt} \delta\nu(t) = F(t) - (1/\tau)\delta\nu(t) \quad (3)$$

Equation 3 is an Ornstein–Uhlenbeck process, where the noise  $F(t)$  is Gaussian white noise with zero mean that satisfies  $\langle F(t)F(0) \rangle = (2\Delta^2/\tau)\delta(t)$ .

The result is that for finite  $N$  the line-broadening dynamics in the subensemble are related to the  $N$ -dependent average

$$G_N(t) = \frac{1}{N} \sum_{i=1}^N \exp(-i \int_0^t ds \delta\nu_i(s)) \quad (4)$$

where  $\delta\nu_i(t)$  is a stochastic realization of the frequency fluctuations according to numerical solutions to eq 3. Figure 4 shows the response function for different values of the Kubo

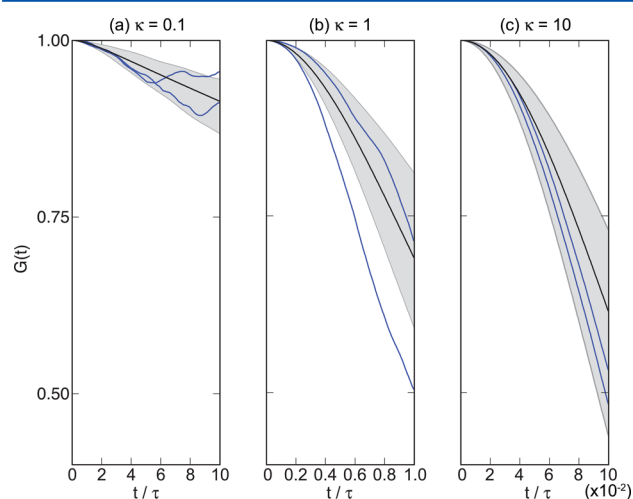


**Figure 4.** Simulating number fluctuations in the free induction decay for subensembles with various values of the Kubo parameter: (a)  $\kappa = 0.1$  (fast modulation limit), (b)  $\kappa = 1$  (intermediate), and (c)  $\kappa = 10$  (slow modulation limit). The solid black curve denotes the ensemble-averaged result and the blue lines are individual stochastic trajectories from a subensemble of 10 oscillators according to eq 3. The Fourier transforms of these data yield spectra, and the broadening of those spectra relate directly to the decay profile of  $G(t)$  through eq 1. The shaded region of the graph gives the standard deviation between the subensemble of 10 oscillators and the ensemble-averaged  $G(t)$ . The size of this region decreases as  $\sim 1/\sqrt{N}$  so that by the time  $N = 1000$  oscillators, the results for the finite system have converged to those of an ensemble where  $N \rightarrow \infty$ . By the estimates given here for the number of oscillators probed, number fluctuations do not account for the variances in experimental line widths reported in Figure 3.

parameter,  $\kappa = \Delta\tau$ . We use the Euler–Maruyama method<sup>35</sup> to approximate the integration of eq 3. The initial stochastic frequency shift is sampled from a normal distribution with a standard deviation of  $\kappa$ . We see that the results converge to the ensemble limit when at least  $10^3$  to  $10^4$  stochastic trajectories are simulated. For smaller ensembles, fluctuations due to small numbers manifest. Simulations for different Kubo parameters do not change these results qualitatively, even into the fast modulation limit. These calculations suggest that for the small ensemble regime probed in these experiments, the large variation in line widths cannot be explained by number fluctuations.

In general, structural variations within the sample, for example, changes in density, can lead to correlated changes in line width and peak position;<sup>14</sup> however, the different dephasing times observed even for the same peak position in our measurements (Figure 3b) suggest that the variations in observed line widths are instead due to dynamical differences in the local chemical environments. A possible mechanism would be alterations in the coupling to low-energy exchange modes, which could modify the pathways for dephasing.<sup>36,37</sup> Further studies on a well-defined and ordered molecular system and under variable temperature conditions would enable us to resolve open questions associated with the contributions of inter- and intramolecular coupling, localization of excitations, and the spectral distribution function of the bath.

In summary, we have directly probed the ultrafast coherent dynamics of molecular subensembles using ultrafast IR nanospectroscopy. We reveal qualitatively novel features of vibrational dynamics in disordered media, directly probing the distribution of dynamical environments in subensembles in real space and revealing variations in chemical environments, both static and dynamic, that occur over nanoscale distances.

The ability to probe nanoscopic local environments is important to understanding complex coherence behavior within, for example, light harvesting and biological systems.<sup>38</sup> The dynamics of energy transfer are closely related to details of aggregation, conformation, and delocalization of excitations.<sup>39</sup> With this spatially resolved coherent spectroscopic approach, it will be possible to study the impact of structure and morphology on molecular interactions, approaching the single-molecule limit.<sup>40,41</sup>

## EXPERIMENTAL METHODS

Excitation is provided by a 76 MHz Ti:Sa oscillator (Coherent, MiraHP) pumping an optical parametric oscillator (OPO, APE) to produce signal and idler in the 1 to 2  $\mu\text{m}$  wavelength range. These two outputs are then used for difference frequency generation (DFG) in GaSe to produce mid-IR light tunable over a broad range from 2 to 12  $\mu\text{m}$ , with  $\sim 200$  fs pulses and transform-limited 50–100  $\text{cm}^{-1}$  bandwidth.

The DFG pulses are directed into an interferometer with 50:50 BaF<sub>2</sub> beamsplitter (BS), with one arm containing the AFM (Attocube) and a reference arm with movable delay  $\Delta t$  and compensation plate (CP) to balance dispersion. This configuration is equivalent to an asymmetric or dispersive Fourier transform spectrometer,<sup>42</sup> which provides additional attenuation information in comparison with conventional Fourier transform spectroscopy. Furthermore, in an *s*-SNOM implementation this configuration is preferable to the symmetric FTIR due to the amplification of the near-field signal with the reference arm.<sup>12</sup>

The AFM is operated in dynamic contact mode, using platinum-silicide coated tips (PtSi-NCH, Nanosensors) with a resonance frequency  $\Omega \approx 300$  kHz. The light is focused onto the AFM tip with a 90° off-axis parabolic mirror (effective focal length 25 mm, effective NA = 0.25), with focus size of  $\sim 20$   $\mu\text{m}$ . The average intensity at the focus is  $\sim 500$   $\text{W}/\text{cm}^2$ . The polarization is along the tip-shaft. The backscattered light from the tip–sample region is then interferometrically heterodyned with the field from the reference arm, with delay  $\Delta t$ , and detected by a HgCdTe detector (MCT, Kolmar). We demodulate the signal at higher harmonics of the cantilever oscillation ( $2\Omega$ ,  $3\Omega$ ...) using a lock-in amplifier (Zurich Instruments, HF2) to extract the near-field response from far-

field background signal. Multiple harmonics of the optical signal, in addition to topographic information, are recorded simultaneously.

## ASSOCIATED CONTENT

### Supporting Information

This material is available free of charge via the Internet The Supporting Information is available free of charge on the ACS Publications website at DOI: 10.1021/acs.jpcllett.5b02093.

Additional data including approach curves, higher harmonics of cantilever oscillation, spatial information, and description of modeling. (PDF)

## AUTHOR INFORMATION

### Corresponding Authors

\*J.M.A.: E-mail: [jatkin@live.unc.edu](mailto:jatkin@live.unc.edu).

\*M.R.: E-mail: [markus.raschke@colorado.edu](mailto:markus.raschke@colorado.edu).

### Notes

The authors declare no competing financial interest.

## ACKNOWLEDGMENTS

J.M.A., P.M.S., and M.B.R. acknowledge support through a partner proposal with the Environmental Molecular Sciences Laboratory (EMSL), a national scientific user facility from the DOE Office of Biological and Environmental Research at Pacific Northwest National Laboratory (PNNL). PNNL is operated by Battelle for the U. S. DOE under Contract DEAC06-76RL01830. J.M.A. and M.B.R. also thank the National Science Foundation (NSF grant No. CHE1306398) for funding. J.D.E. and P.E.T. acknowledge the Donors of the American Chemical Society Petroleum Research Fund for support of this research through award 53301-ND6. We also thank Eric Muller and Honghua Yang for valuable discussion.

## REFERENCES

- (1) Rosenfeld, D. E.; Gengeliczki, Z.; Smith, B. J.; Stack, T. D. P.; Fayer, M. D. Structural dynamics of a catalytic monolayer probed by ultrafast 2D IR vibrational echoes. *Science* **2011**, *334*, 634–9.
- (2) Barbour, L. W.; Hegadorn, M.; Asbury, J. B. Watching electrons move in real time: Ultrafast infrared spectroscopy of a polymer blend photovoltaic material. *J. Am. Chem. Soc.* **2007**, *129*, 15884–15894.
- (3) Tokmakoff, A.; Fayer, M. D. Homogeneous vibrational dynamics and inhomogeneous broadening in glass-forming liquids: Infrared photon echo experiments from room temperature to 10 K. *J. Chem. Phys.* **1995**, *103*, 2810–2826.
- (4) Wernet, P. Electronic structure in real time: mapping valence electron rearrangements during chemical reactions. *Phys. Chem. Chem. Phys.* **2011**, *13*, 16941–16954.
- (5) Son, H.; Park, K.-H.; Kwak, K.-W.; Park, S.; Cho, M. Ultrafast intermolecular vibrational excitation transfer from solute to solvent: Observation of intermediate states. *Chem. Phys.* **2013**, *422*, 37–46.
- (6) Guyot-Sionnest, P. Coherent processes at surfaces: Free-induction decay and photon echo of the Si-H stretching vibration for H/Si(111). *Phys. Rev. Lett.* **1991**, *66*, 1489–1492.
- (7) Paeng, K.; Kaufman, L. J. Single molecule rotational probing of supercooled liquids. *Chem. Soc. Rev.* **2014**, *43*, 977.
- (8) Richert, R. Probing liquid dynamics, one molecule at a time. *Proc. Natl. Acad. Sci. U. S. A.* **2015**, *112*, 4841–4842.
- (9) Zenhausern, F.; Martin, Y.; Wickramasinghe, H. K. Scanning interferometric apertureless microscopy: Optical imaging at 10 Angstrom resolution. *Science* **1995**, *269*, 1083–1085.
- (10) Knoll, B.; Keilmann, F. Near-field probing of vibrational absorption for chemical microscopy. *Nature* **1999**, *399*, 134.

- (11) Huth, F.; Schnell, M.; Wittborn, J.; Ocelic, N.; Hillenbrand, R. Infrared-spectroscopic nanoimaging with a thermal source. *Nat. Mater.* **2011**, *10*, 352–356.
- (12) Bechtel, H. A.; Muller, E. A.; Olmon, R. L.; Martin, M. C.; Raschke, M. B. Ultrabroadband infrared nanospectroscopic imaging. *Proc. Natl. Acad. Sci. U. S. A.* **2014**, *111*, 7191–7196.
- (13) Amarie, S.; Zaslansky, P.; Kajihara, Y.; Griesshaber, E.; Schmahl, W. W.; Keilmann, F. Nano-FTIR chemical mapping of minerals in biological materials. *Beilstein J. Nanotechnol.* **2012**, *3*, 312–323.
- (14) Pollard, B.; Muller, E. A.; Hinrichs, K.; Raschke, M. B. Vibrational nano-spectroscopic imaging correlating structure with intermolecular coupling and dynamics. *Nat. Commun.* **2014**, *5*, 3587.
- (15) Berweger, S.; Nguyen, D. M.; Muller, E. A.; Bechtel, H. A.; Perkins, T. T.; Raschke, M. B. Nano-chemical infrared imaging of membrane proteins in lipid bilayers. *J. Am. Chem. Soc.* **2013**, *135*, 18292–18295.
- (16) Wagner, M.; et al. Ultrafast and Nanoscale Plasmonic Phenomena in Exfoliated Graphene Revealed by Infrared Pump-Probe Nanoscopy. *Nano Lett.* **2014**, *14*, 894–900. PMID: 24479682.
- (17) Eisele, M.; Cocker, T. L.; Huber, M. A.; Plank, M.; Viti, L.; Ercolani, D.; Sorba, L.; Vitiello, M. S.; Huber, R. Ultrafast multi-terahertz nano-spectroscopy with sub-cycle temporal resolution. *Nat. Photonics* **2014**, *8*, 841–845.
- (18) Masetti, G.; Cabassi, F.; Morelli, G.; Zerbi, G. Conformational order and disorder in poly(tetrafluoroethylene) from the infrared spectrum. *Macromolecules* **1973**, *6*, 700–707.
- (19) Wang, C.; Duscher, G.; Paddison, J. Electron energy loss spectroscopy of polytetrafluoroethylene: experiment and first principles calculations. *Microscopy* **2014**, *63*, 73.
- (20) Serov, A.; Choukourov, A.; Melnichuk, I.; Shelemin, A.; Kuzminova, A.; Kylián, O.; Hanus, J.; Kousal, J.; Drábik, M.; Slavínská, D.; Biederman, H. Poly(tetrafluoroethylene) sputtering in a gas aggregation source for fabrication of nano-structured deposits. *Surf. Coat. Technol.* **2014**, *254*, 319.
- (21) Quarti, C.; Milani, A.; Castiglioni, C. Ab initio calculation of the IR spectrum of PTFE: Helical symmetry and defects. *J. Phys. Chem. B* **2013**, *117*, 706–718.
- (22) Xu, X. G.; Rang, M.; Craig, I. M.; Raschke, M. B. Pushing the sample-size limit of infrared vibrational nanospectroscopy: From monolayer toward single molecular sensitivity. *J. Phys. Chem. Lett.* **2012**, *3*, 1836.
- (23) Xu, X. G.; Raschke, M. B. Near-field infrared vibrational dynamics and tip-enhanced decoherence. *Nano Lett.* **2013**, *13*, 1588.
- (24) McLeod, A. S.; Kelly, P.; Goldflam, M. D.; Gainsforth, Z.; Westphal, A. J.; Dominguez, G.; Thiemens, M. H.; Fogler, M. M.; Basov, D. N. Model for quantitative tip-enhanced spectroscopy and the extraction of nanoscale-resolved optical constants. *Phys. Rev. B: Condens. Matter Mater. Phys.* **2014**, *90*, 085136.
- (25) Muller, E. A.; Pollard, B.; Raschke, M. B. Infrared chemical nano-imaging: Accessing structure, coupling, and dynamics on molecular length scales. *J. Phys. Chem. Lett.* **2015**, *6*, 1275–1284.
- (26) Kravtsov, V.; Berweger, S.; Atkin, J. M.; Raschke, M. B. Control of plasmon emission and dynamics at the transition from classical to quantum coupling. *Nano Lett.* **2014**, *14*, 5270.
- (27) Aeschlimann, M.; Brixner, T.; Fischer, A.; Kramer, C.; Melchior, P.; Pfeiffer, W.; Schneider, C.; Strueber, C.; Tuchscherer, P.; Voronine, D. V. Coherent two-dimensional nanoscopy. *Science* **2011**, *333*, 1723–1726.
- (28) Clark, E. S. The crystal structure of polytetrafluoroethylene, forms I and IV. *J. Macromol. Sci., Part B: Phys.* **2006**, *45*, 201–213.
- (29) Clark, E. The molecular conformations of polytetrafluoroethylene: forms II and IV. *Polymer* **1999**, *40*, 4659–4665.
- (30) Kubo, R. The fluctuation-dissipation theorem. *Rep. Prog. Phys.* **1966**, *29*, 255.
- (31) Zwanzig, R. *Nonequilibrium Statistical Mechanics*; Oxford University Press, Oxford, U.K., 2001.
- (32) Nitzan, A. *Chemical Dynamics in Condensed Phases*; Oxford University Press, Oxford, U.K., 2006.
- (33) Weiss, U. *Quantum Dissipative Systems*; World Scientific: Singapore, 1993.
- (34) Barkai, E.; Jung, Y.; Silbey, R. Theory of single-molecule spectroscopy: Beyond the ensemble average. *Annu. Rev. Phys. Chem.* **2004**, *55*, 457–507.
- (35) Higham, D. J. An algorithmic introduction to numerical simulation of stochastic differential equations. *SIAM Rev.* **2001**, *43*, 525.
- (36) Harris, C. B.; Shelby, R. M.; Cornelius, P. A. Effects of energy exchange on vibrational dephasing times in Raman Scattering. *Phys. Rev. Lett.* **1977**, *38*, 1415.
- (37) Rector, K. D.; Fayer, M. D. Vibrational dephasing mechanisms in liquids and glasses: Vibrational echo experiments. *J. Chem. Phys.* **1998**, *108*, 1794.
- (38) Hildner, R.; Brinks, D.; van Hulst, N. F. Femtosecond coherence and quantum control of single molecules at room temperature. *Nat. Phys.* **2011**, *7*, 172–177.
- (39) Brixner, T.; Stenger, J.; Vaswani, H.; Cho, M.; Blankenship, R.; Fleming, G. Two-dimensional spectroscopy of electronic couplings in photosynthesis. *Nature* **2005**, *434*, 625–628.
- (40) Yampolsky, S.; Fishman, D. A.; Dey, S.; Hulkko, E.; Banik, M.; Potma, E. O.; Apkarian, V. A. Seeing a single molecule vibrate through time-resolved coherent anti-Stokes Raman scattering. *Nat. Photonics* **2014**, *8*, 650–656.
- (41) Brinks, D.; Hildner, R.; van Dijk, E. M. H. P.; Stefani, F. D.; Nieder, J. B.; Hernando, J.; van Hulst, N. F. Ultrafast dynamics of single molecules. *Chem. Soc. Rev.* **2014**, *43*, 2476–2491.
- (42) Birch, J. R. Dispersive Fourier-transform spectroscopy. *Microchim. Acta* **1987**, *93*, 105–122.